Croatian Society for Materials Protection

Metalurgija/Metallurgy

Vol. 65 No. 3 / 2026

Multicomponent silicon chromium alloys as an innovative metallurgical reducer

Sławomir Kozłowski [1,*], Bolesław Machulec [2], Wojciech Bialik [2], Stanisław Gil [2] and Grzegorz Pelon [3]

https://doi.org/10.64486/m.65.3.5

[1] Re Alloys sp. z o.o., Łaziska Górne, Poland; slawomir.kozlowski@realloys.pl
[2] Silesian University of Technology, Gliwice, Poland; boleslaw.machulec@polsl.pl wojciech.bialik@polsl.pl, stanislaw.gil@polsl.pl
[3] State Mining Authority, Katowice, Poland; grzegorzpelon@wp.pl
* Correspondence: slawomir.kozlowski@realloys.pl

Type of the Paper: *Article*
Received: August 28, 2025
Accepted: January 5, 2026

Abstract: This publication presents the results of modelling physicochemical processes in a submerged arc furnace for melting silicon-iron-chromium alloys characterized by a Cr/Fe ratio of at least 2.0. The refining of these alloys by metallurgical decarburization is also discussed, reducing the C content to a maximum of 0.02 % by weight. These alloys are used as new chromium ore reducers in the production of low-carbon ferrochrome. A physicochemical model developed before trial production of the alloys enabled the determination of key parameters of the technological process and the definition of their allowable ranges of variability. The developed model was verified through its implementation into metallurgical practice at the ReAlloys sp. z o.o. ferroalloys plant. It was determined that, provided appropriate technological procedures were maintained, the deviations between the parameters calculated in the model and those obtained during production did not exceed 3 %.

Keywords: ferroalloys; carbothermic reduction; low carbon ferrochrome

1. Introduction

Production procedures and the effect of mineral admixtures on structure and properties are currently attracting significant research interest due to the use of carbon-based reducing agents, which contribute to overall CO_2 emissions in metallurgical processes. Ferrochrome is the primary source of chromium used in modern Cr-containing alloys. Most of its production is used in high-alloy steels, which owe their corrosion and high-temperature resistance primarily to their Cr and Ni content.

Sommerfeld et al. investigated the possibility of replacing fossil coke with silicon-rich waste for ferrochrome production in an electric arc furnace. Due to the highly exothermic reaction of silicon with iron and chromium oxides, silicothermal reduction resulted in a reduction in specific electrical energy consumption compared to carbothermal reduction [1]. Li et al. conducted research on the processing and properties of FeSiCr powders, techniques for processing and stabilizing these powders, and their behavior as reducing agents in melting [2]. Makhambetov et al. analyzed a metallothermic process for producing chromium-manganese (Cr-Mn) ligatures from low-grade ores, using silicon-aluminum alloys as reducing agents, which are important for the design of multicomponent reducing agents containing Si and Cr. The results showed that the reducing agent used (aluminosilicate manganese (AlSiMn) or ferrosilicate aluminum

(FeSiAl)) produced ligatures with varying compositions; for example, the AlSiMn-based product contained 53.74 % Cr, 20.03 % Mn, and 3.06 % Si [3].

Akhmetov et al. experimented with the production of carbon-free ferrochrome using a metallothermic smelting method with a complex FeAlSiCa alloy as the reducing agent. This technique is intended to provide an alternative to traditional carbon-based methods, reducing carbon footprint and emissions. It was found to achieve high Cr recovery (up to 80 %) and meet the requirements for low-emission ferrochrome under optimal conditions [4]. Du Preez et al. reviewed and summarized the various processes currently used in the South African FeCr industry and identified wastes at each stage of the process. They identified various management systems that could be improved, including utilizing the energy associated with combustion of CO-rich exhaust gases, using an alternative low-temperature chromite pelletization process, and considering the potential of hydrogen as a chromite reducer [5]. Zhang et al. studied the solubility of nitrogen in superduplex or hyperduplex stainless steel, which is characterized by very high Cr content, as well as the activity interaction parameters between N and other alloying elements. Experimental results showed that N solubility increased significantly with increasing Cr content, reaching over 1 wt % at Cr contents of approximately 40 wt % [6].

Li et al. considered the efficiency of the smelting process of a semi-steel converter containing chromium and its dependence on the slag formation rate in the initial stage of the converter. The effect of Cr2O3 content on the physicochemical properties of the $CaO{\cdot}SiO_2$–FeO–MgO system, such as melting point, solidification behavior, mineral composition, and lime dissolution rate, was investigated. The results showed that the slag was an amorphous phase at 1500°C. After adding Cr_2O_3, $Ca(Fe,Mg)Si_2O_6$ and spinels were formed in the slag. As the Cr_2O_3 content increased, the amount of spinel precipitation increased, and the dendritic Fe3O4 crystal gradually transformed into a granular $(Fe,Mg)(Fe,Cr)_2O_4$ crystal [7].

Abdirashit et al. presented the results of laboratory studies on the smelting of nickel-chromium ferroalloys from low-grade nickel ores from Kazakhstan. X-ray phase analysis was performed on raw materials, which included quartz, nontronite, chromium metahydroxide, goethite, magnetite, ferrous chromite, and nickel(II) silicate. Reduction reactions of metal oxides with carbon and carbon monoxide with increasing temperature were investigated. The results of these studies confirmed the feasibility of producing a nickel-chromium alloy with nickel contents of (2–10) % and chromium contents of (2–7) % [8].

Shi et al. presented an experimental paper on the use of silicon-containing materials for the direct reduction of chromite and the introduction of Si into steel. This research was crucial for the concept of silicothermal use of Si–Cr alloys [9].

The process of smelting silicon alloys with the addition of iron or with iron and chromium in electric submerged arc furnaces is a continuous process [10–12]. The charge is introduced into the furnace from the top and consists of a mixture of quartzite, carbon-based reducing materials (such as hard coal, wood chips, and sometimes charcoal), and iron carriers (e.g. mill scale or steel chips).

In the production of ferrosilicon-chromium (FeSiCr) alloys, the amount of iron charge additions is limited, and the main source of chromium is high-carbon ferrochromium. The liquid metal is periodically tapped into the ladle through a special opening located in the side wall of the furnace bath, right next to the furnace hearth. The energy required for the highly endothermic silica reduction reactions comes from two sources: resistance heating (current flowing directly through the charge) and thermal radiation emitted by an electric arc, which glows in gas chambers near the electrodes. View of the three-electrode furnace (figure 1) is presented below.

The efficiency of the SiO_2 reduction process depends largely on the thermal and energy conditions prevailing in the reaction zones located near the electrodes. Although this process is classified as non-slag, in practice it always produces a small amount of slag. This is due to the quality of the raw materials used and the presence of trace amounts of oxides (such as Al_2O_3, CaO, MgO, TiO_2) present in quartzites and ash derived from carbon reduction materials.

https://doi.org/10.64486/m.65.3.5

Figure 1. View of the three-electrode furnace (author's own work)

FeSiCr alloys containing up to 50 % silicon are commonly produced in the ferroalloy industry. Depending on the silicon content, they are used as reducing agents in the silicothermic production of medium- and low-carbon ferrochrome, as well as deoxidizers and alloying additives in the production of low-alloy and alloy steels. In these applications, the key functional characteristics of FeSiCr alloys are their reducing potential related to the silicon content and the strongly exothermic nature of silicothermic reactions, which can support the reduction of chromium oxides and thereby improve process efficiency compared with purely carbothermic routes [1,5,9]. For the specific application as a reducer in low-carbon ferrochrome production, it is also important to limit the introduction of undesired elements; therefore, alloys with ultra-low carbon are preferred to avoid carbon pickup in downstream processing. Moreover, a sufficiently high Cr/Fe ratio is required to minimize iron dilution when the alloy is used as a chromium ore reducer and to support achieving the target chromium grade in the final product.

Until recently, FeSiCr alloys with increased silicon content (≥ 61 wt. %), chromium (≥ 21 wt. %), low carbon content (≤ 0.02 wt. %), and a Cr:Fe ratio of at least 2.0 were not produced in the Polish ferroalloys industry [13]. Production of these high-quality alloys was initiated in 2023 at Re Alloys sp. z o.o. as part of efforts to increase the efficiency and innovation of the technological process. The process utilized a previously developed physicochemical model for melting Fe-Si-Cr alloys in submerged arc furnaces, described in [14]. This model is an extension of the earlier two-reactor models of ferrosilicon melting [14–17], extended by two additional reactors: the first one for heating the charge with post-reaction gases generated during silica reduction and decomposition of volatile components of carbon reductants, and the second one for combustion of post-reaction gases with atmospheric air under the furnace hood. In the analysis of enthalpy changes of volatile components of reductants, empirical relations concerning specific heat [18] were used, distinguishing between primary volatile fractions (released at lower temperatures) and secondary volatile fractions (released at higher temperatures).

The objective of the paper was to present the results of modelling physicochemical processes in a submerged arc furnace for melting silicon-iron-chromium alloys characterized by a Cr/Fe ratio of at least 2.0.

2. Physicochemical basics of silicon alloy melting

One of the most important structural elements of a submerged arc furnace's workspace are carbon electrodes immersed in the charge, through which electric current is supplied to the furnace's workspace. The conversion of electrical energy into heat occurs in a combined manner in solid, liquid, and gaseous media [15–17], and the temperature and electric fields are coupled. The electrodes form reaction zones, the size of which depends on their diameter. View of the modelled temperature field of reaction zones around electrodes (figure 2) is presented below.

https://doi.org/10.64486/m.65.3.5

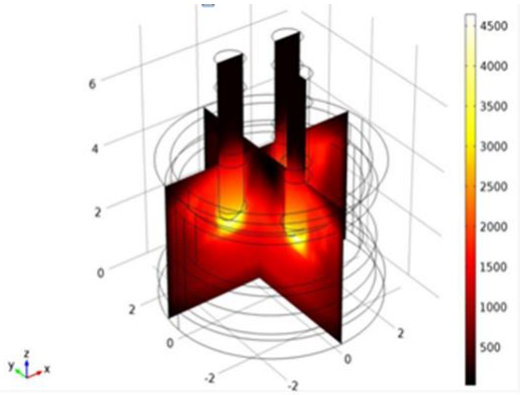

Figure 2. Modelled temperature field of reaction zones around electrodes (temperature in Kelvin) (author's own work)

These are areas where current flows, heat is released, and the charge is in constant motion. Considering the heat release mechanism, physicochemical and electrical models of submerged arc furnaces distinguish between two zones:

- the charge zone, where heat is released because of resistive heating,
- the interior and walls of the arc gas chamber, where heat is released because of the arc's thermal radiation.

The rate of silica melting, the course of physicochemical processes, and the internal structure of the furnace are closely related to the temperature conditions of the reaction zones and the proportions of heat released in both zones. In the present work, these thermal conditions were represented by the characteristic temperatures of the modelled reaction zones: T_1 = 1630 °C (upper zone) and T_2 = 1930 °C (high-temperature lower zone near the electrode tips) [10–12]. These proportions should be consistent with the energy balance of the physicochemical processes occurring there under conditions that maximize silicon yield. These proportions are closely related to the geometric and electrical parameters of the furnace [19], the electrode position, and the electrical properties of the charge mixture. Due to the burning process, the electrodes should be systematically extended. The granulometric composition of the charge, particularly the granulometric composition of the carbon reducers, has a significant impact on heat distribution and the temperature conditions of the reaction zones. This effect results from changes in bed permeability and gas flow (which influence convective heat transfer and the removal/recirculation of reaction gases), the electrical resistivity and current paths in the burden (which control the share of resistive heating in the charge zone and the development of the arc cavity), and the available reactive surface area of carbon (affecting the kinetics of reactions such as SiO consumption and intermediate SiC formation). Consequently, variations in reducer particle size distribution may shift the location and intensity of heat generation and alter the temperature field in the vicinity of the electrodes [11,12,14,15]. Optimal electrode positioning and correct temperature conditions of the process lead to minimized raw material and energy consumption and maximized Si yield.

The process of reducing silica with carbon produces SiO(g) as an intermediate product, which forms in the highest-temperature zones of the furnace located near the electrode ends (represented in the model by T_2 = 1930 °C) [10–12]. Simultaneously, SiO(g) formation is accompanied by reactions that produce metallic silicon [10–12]. A portion of the gaseous SiO(g) migrates upward and reacts with carbon in cooler regions of the charge (represented by T_1 = 1630 °C), leading to the formation of intermediate products such as SiC [10–12]. The refractory SiC carbide descends with the partially reacted charge to the bottom of the furnace. In the highest-temperature zones (T_2), it is consumed in reactions that generate SiO(g) and silicon [10–12]. The SiC formation reaction can also occur in lower-temperature zones (T_1), involving previously unreacted carbon [10–12]. The physicochemical conditions for the SiO(g) condensation reaction have a significant impact on silicon yield and the efficiency of the electrothermal silica reduction process [10–12]. The SiO(g)–carbon reaction slows down as the reducer surface becomes covered with carbide, and its course is significantly influenced by the

https://doi.org/10.64486/m.65.3.5

reactivity of the reducers [10–12]. SiC carbide, an intermediate product of the silica–carbon reduction process, has a significant impact on the electrical properties of the current-carrying zones and the resistance of the furnace bath due to its low resistivity at high temperatures [10–12]. Its deposition in the furnace is closely related to the heat distribution in the reaction zones and the temperature conditions of the process [10–12].

Assuming equilibrium conditions in the charge preheating zone, as in the other zones, is a significant simplification, but it enables thermochemical calculations using the Gibbs free energy minimization algorithm [20,21] and allows for determining the influence of key factors on the physicochemical conditions of the silicon alloy melting process in submerged arc furnaces. The procedure consists of: defining the set of possible phases/species and the elemental composition of the feed, performing Gibbs energy minimization to obtain the equilibrium composition at T_1 and T_2, and updating the system streams in an iterative cycle to represent the continuous process (workflow shown in Figures 4 and 5). Under real conditions, the thermal-chemical equilibrium temperature can be approximated by the off-gas temperature measured just above the charge surface. In this work, this temperature was represented by T0 = 753.4 °C, obtained from the mass and heat balance (figure 4), which is consistent with typical off-gas temperature levels reported for submerged arc furnaces [10–12].

3. Equilibrium model of the silicon alloy melting process in Fe-Si-Cr-O-C-Al-Ca-Mg-Ti system

The physicochemical model of the silica reduction process with carbon was adopted as a system consisting of two closed isothermal reactors [12,14,21]: the upper reactor with a lower temperature T_1 (1630 °C) and the lower reactor with a higher temperature T_2 (1930 °C). Cyclic mass exchange occurs between the reactors and the environment, as well as between the reactors within the system, when equilibrium is reached in the reactors. The role of T_1 and T_2 in the model and the dominant reaction pathways assumed in each reactor are illustrated in figure 3.

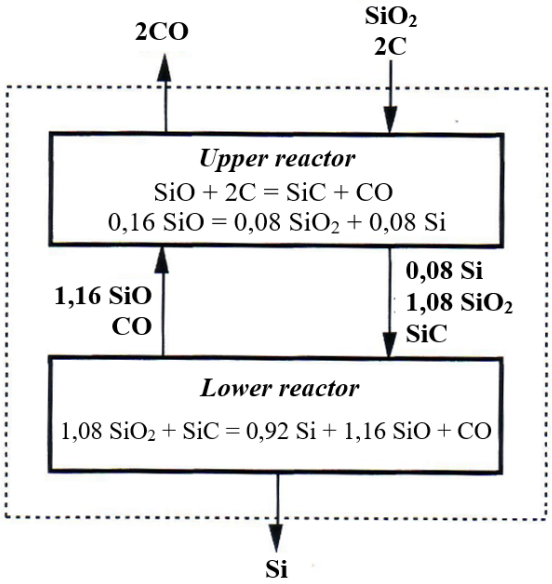

Figure 3. Main reactions assumed in the two-reactor model at T_1 = 1630 °C (SiC formation zone) and T_2 = 1930 °C (SiO generation zone) (author's own work)

In the upper reactor (T_1), representing the cooler zone of the furnace charge, the formation of intermediate silicon carbide (SiC) is accounted for. In the lower reactor (T_2), representing the high-temperature reaction zone near the electrode tips, the generation of gaseous silicon monoxide SiO(g) is dominant and governs the overall reduction mechanism and silicon yield. The continuous silicon alloy smelting process was simulated recursively. Additionally, the model includes two additional reactors in which processes related to cooling the post-reaction gases from the silica reduction process with carbon and their post-combustion with atmospheric

https://doi.org/10.64486/m.65.3.5

air take place. In cycle 1, a portion of the reaction mixture is introduced into the upper reactor, the molar composition of which corresponds to the composition of the feed mixture in the silicon alloy smelting process, calculated per 1 kmol of SiO_2. Chemical reactions occur in the lower reactor until equilibrium is reached at temperature T_1. The gas-phase products then leave the lower reactor and enter the upper reactor, where they cool to temperature T_0 (753.4 °C), transferring heat to the cold charge entering the next process cycle (figure 4).

Raw material	kg	kg/t	**Gases**	kmol	kg/t
FeCrHC	100	344,03	CO(g)	1,247	988,15
Quartzite	500	1720,15	CO_2(g)	0,310	386,06
Mill scale	10	34,40	CH_4(g)	0,942	427,52
Wood chips	120	413,46	H_2O(g)	0,605	308,34
Coal Poland	100	344,03	Total	3,104	2110,07
Coal Colombia	190	653,66	Soot	kmol	kg/t
Steel bars	3,5	12,04	C	0,397	134,97
Electrode casing	1,0	3,46	**Dust**	kmol	kg/t
Electrode paste	10,2	34,97	SiO_2	0,087	147,42
Total		**3560,19**	$MgSiO_3$	0,0002	0,66
			Total		148,223

Cycle 40 P = 1bar **T_0 = 753,4 °C**

Reactor 0, Pre-heating the batch to T_0

Energy balance		Mcal/kmol	kWh/t
Energy of devaluation of charge components		1,219	40,09
Decomposition of secondary volatiles		5,92	194,78
Evaporation and change of H_2O entalphy	ΔH_{25}^{T0}	10,289	338,26
Enthalpy change of volatiles		6,225	204,64
Enthalpy change of charge components		18,96	623,18
Cooling down gas from Reactor 1	ΔH_{T1}^{T0}	-15,711	-516,53
The heat effect in Reactor 0	$\Delta H_R(T_0)$	-26,902	-884,43
	Total	0,000	0,000

Component	kmol	**Component**	kmol	**Gases**	kmol	kg/t
FeO	0,01645	Cr2O3	0,00040	CO(g)	1,9544	1548,50
Fe2O3	0,00415	TiO2	0,00063	CO2(g)	0,0002	0,19
SiO2	1	H2O	0,60506	Mg(g)	0,0002	0,16
Al2O3	0,00532	Fe	0,05422	SiO(g)	0,0868	108,30
CaO	0,00309	Cr	0,15655			
MgO	0,00228	C	2,07180			

Figure 4. Calculated mass and heat balance in reactor 0 (author's own work)

Under actual conditions, temperature T_0 approximately corresponds to the temperature of the byproduct gases in the silica reduction process with carbon immediately after leaving the furnace, just at the top of the charge. Simultaneously, the condensed-phase products from the lower reactor migrate downward, where they react with each other until equilibrium is reached at temperature T_2. The condensed-phase products then leave the reactor and, after cooling to the tapping temperature, form a metallic and slag phase, leaving the system and not participating in further processing. Simultaneously, the gas-phase products with equilibrium

https://doi.org/10.64486/m.65.3.5

composition leave the reactor and, after cooling to temperature T_1, are reintroduced into the lower reactor, where they react in the next cycle of the reaction system (figure 5).

Cycle 40	**P=1 bar**	**E=4237,207**	**kWh/Mg**	**T_1=**	**1630**	**°C**
			Reactor 1			
Component	kmol	Component	kmol		Component	kmol
SiC	0,5908	CrSi	0,068		CO(g)	0,4924
SiO_2	0,2826	CrSi2	0,038		SiO(g)	0,2472
Al_2O_3	0,0030	MgSiO3	0,047		Si2O2(g)	0,0002
$CaSiO_3$	0,0013	Fe	0,009		Si(g)	0,0002
Cr	0,0145	FeSi	0,067		Ca(g)	0,0003
Cr_3C_2	0,0067	Si	0,021		Mg(g)	0,0539
Cr_4C	0,0036					
	P=1 bar	**E=2351,29**	**kWh/Mg**	**T_2=**	**1930**	**°C**
			Reactor 2			
Yield	Metal	kmol	wg. %		Slag clot	kg/kmol	kg/Mg
99,99%	Fe	0,0790	12,47		SiC	4,6563	131,72
79,68%	Si	0,7992	63,50		Slag	0,3476	9,83
99,97%	Cr	0,1573	23,13				
47,64%	Al	0,0052	0,39				
	C	0,0004	0,01				
77,47%	Ca	0,0024	0,27				
62,49%	Mg	0,0018	0,12				
100,00%	Ti	0,0007	0,10				
Energy efficiency	**92%**						
Energy indicator	**7161,41 kWh/Mg**						
Metal	**35,352 kg/kmol**						

Figure 5. Mass and heat balance in reactors 1 and 2 (author's own work)

Cycle 2 and each subsequent cycle begin with the introduction of a new portion of the reaction mixture into the lower reactor, which reacts with the remaining gas phase components from the previous cycle until equilibrium is reached at temperature T_1. Subsequent cycles proceed identically to cycle 1.

4. Results

Table 1 summarizes the planned and achieved weighted-average chemical compositions of the alloys obtained during the technological tests. The chemical composition was determined in the Re Alloys plant laboratory using X-ray fluorescence spectrometry (XRF) with a Thermo Fisher Scientific ARL PERFORM'X 4200 spectrometer. The target compositions were achieved for both the major elements (Si, Cr) and the undesired elements (P, C, S). For both FeSi48Cr LC and FeSi60Cr LC alloys, the Cr/Fe ratio exceeded the calculated value of 2.0. In addition, both alloys exhibited slightly higher contents of the major elements and lower impurity levels than assumed.

https://doi.org/10.64486/m.65.3.5

Table 1. Chemical composition of the FeSiCrLC alloys

Element	FeSi48CrLC		FeSi60CrLC	
	calculated	achieved	calculated	achieved
	wt. %			
Si	48.00	48.98	64.00	64.29
Cr	33.00	33.42	22.00	22.72
Fe	16.50	16.32	11.00	10.85
P	0.02	0.011	0.02	0.013
C	0.02	0.019	0.02	0.017
S	0.05	0.002	0.05	0.002

In Table 2 the planned and achieved indicators have been presented during the technological trials. Daily efficiency indicators and the specific electricity consumption indicators were achieved very close to calculated in the physicochemical model. Table 3 presents the planned and achieved raw material consumption. The differences between the planned and actual consumption rates are due to the quality parameters of the raw materials, which, during the market turmoil associated with the crisis caused by the coronavirus pandemic, suppliers were unable to meet. The supplied high-carbon ferrochrome (FeCrHC) was planned to contain 68 % Cr by mass, and during technological tests, the Cr content in FeCrHC was (62–65) % by mass. The supplied coal was also planned to contain 62 % fixed carbon (C_{fix}), i.e., the fraction of carbon remaining after the removal of moisture and volatile matter (proximate analysis) and therefore the portion effectively available for carbothermic reduction reactions of silicon, calcium, and aluminum oxides. Due to the energy crisis and the shortage of hard coal on the domestic market [22,23], Colombian coal containing (44–48) % C_{fix} was used in the process; this Cfix range was determined by proximate analysis performed in the Re Alloys plant laboratory (batch-wise internal quality control for the delivered coal). Due to the lower quality parameters of the input raw materials, the unit consumption rates deteriorated.

Table 2. Summary of production indexes

Alloy FeSiCr		Electricity consumption MWh/Mg	Daily productivity Mg	Refining loss %
FeSi48CrLC	calculated	5.499	33.30	8.0
	achieved	5.906	32.49	10.1
FeSi60CrLC	calculated	7.161	25.00	8.0
	achieved	7.133	25.34	9.7

Table 3. Summary of raw material consumption

Charge material	FeSi48CrLC		FeSi60CrLC	
	calculated	achieved	calculated	achieved
	kg / Mg			
FeCrHC	534	553	325	387
Quartzite	1240	1240	1406	1617
Coal (C_{fix} = 62 %)	-	537	951	-
Coal (C_{fix} = 47 %)	920	215	-	1276
Mill scale	18	16	-	-
Wood chips	260	248	238	323
Electrode paste	40	38	40	47

https://doi.org/10.64486/m.65.3.5

5. Conclusions

During the technological tests to produce the FeSi60CrLC alloy, a daily productivity index of 25.43 Mg was achieved, which is a better result than expected (min. 25 Mg per day), while the electricity consumption index was 7.133 MWh/Mg, which is a better result than expected (max. 7.161 MWh/Mg). Due to the market problems described in the paper, difficulties arose in supplying raw materials of the assumed quality. The supplied high-carbon ferrochrome had a lower Cr content (62-65) % by weight than the high-carbon ferrochrome assumed for use in the FeSiCr alloy production process during the funding application 68 % by weight. The hard coal used during the technological tests also had a lower carbon content (C_{fix} approx. 47 % by weight) than the hard coal from Polish mines assumed in the application (C_{fix} approx. 62 % by weight). These poorer quality parameters resulted in higher unit raw material consumption rates.

During technological tests, a better than expected quality of the FeSi60CrLC alloy was obtained in terms of chemical composition: Cr min. 22 wt. % (weighted average 22.71 wt. %), Si min. 64 wt. % (weighted average 64.19 wt. %), Cr/Fe ratio min. 2.0 (weighted average 2.06) and undesirable elements in the alloy: P max. 0.02 wt. % (weighted average 0.013 wt. %), S max. 0.02 wt. % (weighted average 0.002 wt. %), C max. 0.02 wt. % (weighted average 0.017 wt. %).

The physicochemical model implemented in the industrial activity of the Re Alloys Ltd. Ferroalloys plant showed a deviation between the obtained indices and the calculated ones up to 3 %. Comparison with recent studies. The obtained results support the broader trend of using silicon-containing materials as effective reducers in chromium-bearing systems. Recent studies indicate that silicothermic reactions can contribute to improved process efficiency relative to purely carbothermic routes, due to the strongly exothermic character of silicon oxidation and its role in reducing metal oxides (e.g., Sommerfeld et al. [1]; Shi et al. [9]).

In addition, the development of complex, low-emission routes for ferrochrome production using multicomponent reducers has been reported in recent literature (e.g., Akhmetov et al. [4]), and the need for process optimization and improved resource/energy management in ferrochrome production has been highlighted in industry reviews (e.g., du Preez et al. [5]). In this context, the present work contributes industrial-scale evidence that high-Si FeSiCr alloys with ultra-low carbon can be produced with stable quality and predictable performance, enabling their intended use as innovative reducers for low-carbon ferrochrome production.

Future work. Future research will focus on further optimization of raw material selection and charge preparation (including reducer granulometry and Cfix variability), reduction of specific energy consumption, and broader evaluation of the environmental impact of replacing conventional reductants with high-Si FeSiCr reducers under industrial conditions.

Acknowledgments: This paper is published with the permission of the Re Alloys sp. z o.o. Ferroalloys Plant management. This study is a part of works carried out under the project "Crosimax - an innovative alloy of silicon with chromium, iron, aluminium and calcium, as a versatile and effective reducing agent of increased deoxidising potential towards Cr_2O_3 - to be applied in manufacturing of low and ultra-low carbon grades of ferro-chromium", co-funded by the Polish NCBiR Committee, No.: POIR.01.01.01-00-0161/21 within Operational Programme Smart Growth 2014-2020.

References

[1] M. Sommerfeld, J. Weiss, B. Friedrich, Minimized ferrochrome production utilizing silicon wafer cutting waste, *Journal of Sustainable Metallurgy* vol. 9, 2023, pp. 806–815, https://doi.org/10.1007/s40831-023-00688-z

[2] C. Li , H. Yu, G. Han, Z. Liu, FeSiCr-Based Soft Magnetic Composites with SiO2 Insulation Coating Prepared Using the Elemental Silicon Powder Hydrolysis Method, Metals vol. 13, no. 8, 2023, 1444, https://doi.org/10.3390/met13081444

https://doi.org/10.64486/m.65.3.5

[3] Y. Makhambetov, S. Abdulina, S. Kabylkanov, A. Burumbayev, A. Zhakan, Z. Sadyk, A. Akhmetov, Production of Chromium–Manganese Ligature from Low-Grade Chromium and Iron–Manganese Ores Using Silicon–Aluminum Alloys as Reductants, Processes vol. 13, no. 10, 2025, 3158, https://doi.org/10.3390/pr13103158

[4] A. Akhmetov, Z. Zulhan, Z. Sadyk, A. Burumbayev, A. Zhakan, S. Kabylkanov, R. Toleukadyr, Z. Saulebek, Z. Ayaganova, Y. Makhambetov, Carbon-Free Smelting of Ferrochrome Using FeAlSiCa Alloy, Processes vol. 13, no. 6, 2025, 1745, https://doi.org/10.3390/pr13061745

[5] S.P. du Preez, T.P.M. van Kaam, E. Ringdalen, M. Tangstad, K. Morita, D.G. Bessarabov, P.G. van Zyl, J.P. Beukes, An Overview of Currently Applied Ferrochrome Production Processes and Their Waste Management Practices, Minerals vol. 13, no. 6, 2023, 809, https://doi.org/10.3390/min13060809

[6] J. Zhang, X. Luo, B. Yan, Thermodynamic Study on the Solubility of N in High Cr, Ni and Mo Content Fe-Cr-Ni-Mo-O Melts, Metals vol. 14, no. 12, 2024, 1366, https://doi.org/10.3390/met14121366

[7] S. Li, J. Li, Y. Yu, H. Zhu, Effect of Cr2O3 on properties of CaO–SiO2–FetO–MgO system and dissolution behavior of lime, Journal of Iron and Steel Research International vol. 31, 2024, pp. 870–881, https://doi.org/10.1007/s42243-023-01121-1

[8] A. Abdirashit, B. Kelamanov, O. Sariyev, D. Yessengaliyev, A. Abilberikova, T. Zhuniskaliyev, Y. Kuatbay, M. Naurazbayev, A. Nazargali, Study of Nickel–Chromium-Containing Ferroalloy Production, Processes vol. 14, no. 4, 2025, 1258, https://doi.org/10.3390/pr13041258

[9] C. Shi, Z. Li, Y. Liu, Y. Kobayashi, Activity of Chromium Oxide in CaO–SiO2–MgO–Al2O3–MnO–CaF2–CrOx Slag for Chromium Reducing Process, ISIJ International vol. 64, no. 6, 2024, pp. 893–900, https://doi.org/10.2355/isijinternational.ISIJINT-2023-214

[10] W. Bialik, S. Gil, T. Pawlik, S. Kozłowski, K. Kołtun, Influence of Admixtures of Mineral Elements in Reducing Agents on the Structure of FeSi and FeSiCr Ferroalloys, Engineering Proceedings vol. 64, no. 1, 2024, 20, https://doi.org/10.3390/engproc2024064020

[11] B. Machulec, S. Gil, W. Bialik, Equilibrium model of the ferrosilicon process in the submerged arc furnace, Proceedings of the METAL 2018, Brno, Czech Republic, 2018, pp. 122–127.

[12] A. Schei, J.K. Tuset, H. Tveit, Production of High Silicon Alloys, Tapir Forlag, Trondheim, Norway, 1998.

[13] S. Kozłowski, Ł. Banasik, Innowacyjne rozwiązania w elektrometalurgii żelazostopów na przykładzie projektów realizowanych przez Re Alloys sp. z o.o. Hutnik-WH, vol. 88, no. 1, 2021, pp. 14–21, https://doi.org/10.15199/24.2021.1.3 (in Polish)

[14] V.I. Zubov, M.I. Gasik, Elektrometallurgy of Ferrosilicon, Physical-Chemistry and Technology. Sistemniye tekhnologii, Dnepropetrovsk, Ukraine, 2002., (in Russian)

[15] N.V. Tolstoguzov, Theoretical foundations and technology of melting silicon and manganese alloys, Metallurgiya, Moscow, Russian Federation, 1992., (in Russian)

[16] B. Andresen, J.K. Tuset, Dynamical model for the high-temperature part of the carbothermic silicon metal process, Proceedings of INFACON 7, Trondheim, Norway, 1995, pp. 535–544.

[17] S.A. Halvorsen, A. Schei, J.H. Downing, A unidimensional dynamic model for the (ferro)silicon process, Proceedings of Electric Furnace Conference, Atlanta, USA, 1992, pp. 45–59.

[18] B. Leśniak, Ł. Słupik, G. Jakubina, Określenie pojemności cieplnej węgla w świetle danych literaturowych, Chemik, vol. 6, 2013, pp. 560–571. [Online] Available: https://bibliotekanauki.pl/articles/1216441.pdf (in Polish). [Accessed: Nov. 10, 2025].

[19] B. Machulec, W. Bialik, Thermal and electrical similarity of reaction zones in the ferrosilicon submerged arc furnace, Modern problems of Metallurgy, vol. 1, 2016, pp. 154–161.

[20] A. Roine, HSC Chemistry 7.0 Users Guide, Outotec Information Center, Pori 2009.

[21] N.K. Batra, Modelling of ferrosilicon smelting in submerged arc furnace, Iron and Steelmaking, vol. 39, no. 5, 2003, pp. 399–404, https://doi.org/10.1179/030192303225004088

[22] A. Gałaś, A. Kot-Niewiadomska, H. Czerw, V. Simić, M. Tost, L. Wårell, S. Gałaś, Impact of Covid-19 on the Mining Sector and Raw Materials Security in Selected European Countries, Resources, vol. 10, no. 39, 2021, https://doi.org/10.3390/resources10050039

[23] A. Chmiela, D. Wójcik, M. Wysocka, Zakłócenia zaawansowania procesów restrukturyzacji, rewitalizacji i likwidacji dużej kopalni węgla kamiennego, wywołane pandemią COVID-19, Systemy Wspomagania w Inżynierii Produkcji, vol. 12, no. 1, 2023, pp. 73–83. [Online] Available: https://yadda.icm.edu.pl/baztech/element/bwmeta1.element.baztech-7a3cdf5f-2792-489b-b64d-666d43ebbc5a/c/07___kopia.pdf (in Polish). [Accessed: Nov. 10, 2025]

https://doi.org/10.64486/m.65.3.5